Three-Dimensional TiO₂/ZnO Hybrid Array as a Heterostructured Anode for Efficient Quantum-Dot-Sensitized Solar Cells

Hao-Lin Feng,[†] Wu-Qiang Wu,[†] Hua-Shang Rao,[†] Quan Wan,[‡] Long-Bin Li,[†] Dai-Bin Kuang,*[,†] and Cheng-Yong Su[†]

†MOE Key Laboratory of Bioinorganic and Synthetic Chemistry, Lehn Institute of Functional Materials, School of Chemistry and Chemical Engineering, Sun Yat-Sen University, Guangzhou 510275, P. R. China
‡Guangzhou Quality Supervision and Testing Institute, Guangzhou 510110, P. R. China

ⓢ *Supporting Information*

ABSTRACT: The development of a novel nanoarray photoanode with a heterostructure on a transparent conducting oxide substrate provides a promising scheme to fabricate efficient energy conversion devices. Herein, we successfully synthesize the vertically aligned hierarchical TiO₂ nanowire/ZnO nanorod or TiO₂ nanowire/ZnO nanosheet hybrid arrays, which are proven to be excellent anode candidates for superior light utilization. Consequently, the quantum-dot-sensitized solar cells based on such hybrid arrays exhibit an impressive power conversion efficiency (PCE) under AM 1.5G one sun illumination with improved short-circuit current density (J_{SC}) and fill factor compared to pristine TiO₂ nanowire arrays. Combined with the chemical-bath-deposited Cu₂S counter electrode, the eventual PCE can be further optimized to as high as 4.57% for CdS/CdSe co-sensitized quantum dot solar cells.

KEYWORDS: *quantum dots, photovoltaic, nanowire arrays, heterostructure, light harvesting*
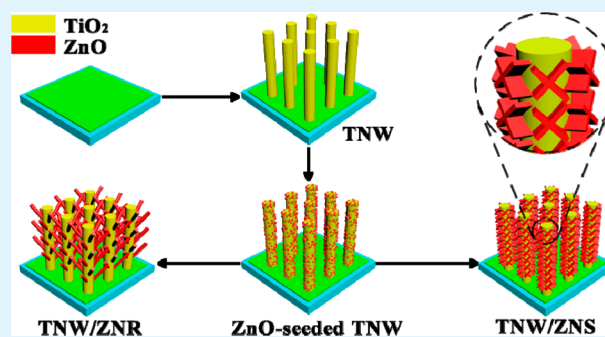
1. INTRODUCTION

In recent years, semiconductor-nanomaterial-driven photovoltaic devices have attracted considerable interest.[1−3] Among all of the photovoltaic devices, dye-sensitized solar cells (DSSCs) have been regarded as the most promising candidate for efficient solar energy conversion owing to their low cost and environmentally benign advantages compared to the traditional silicon-based solar cells.[4−6] In order to enhance the light-harvesting efficiency of DSSCs, much effort has been made to develop new sensitizers, for instance, porphyrin dyes[7] or narrow-band-gap quantum-dot (QD) semiconductors.[8] Specifically, QDs such as CdS,[9,10] CdSe,[11,12] CdTe,[13,14] PbS,[15,16] PbSe,[17] Sb₂S₃,[18] etc., exhibited excellent optical and electronic properties, namely, a tunable band gap upon QD size, high molar extinction coefficient, and generation of multiple electrons,[19−22] which could lead to 44% theoretical photovoltaic conversion in quantum-dot-sensitized solar cells (QDSSCs).[23]

Apart from sensitizers, morphologies and structures of anode materials also played an important role in enhancing the photovoltaic performance of solar cells.[11,24−26] Normally, mesoporous nanoparticle films are widely used as photoanodes in solar cells owing to their high internal surface area for sufficient sensitizer anchoring. However, the enormous defects, surface states, and grain boundaries existing in the random electrical pathway of nanoparticles would lead to many unexpected trapping and detrapping events, thus hindering further improvement of the photovoltaic performance.[9,11] More often than not, poor light utilization, charge-transport rate, and charge collection efficiency are the troublesome issue for nanoparticle-based cells.[13] In contrast, one-dimensional (1D) nanostructures such as nanowires[11,27] and nanotubes[28] have been introduced as photoanodes because of their outstanding features of providing a direct pathway for charge transport and also efficiently suppressing charge recombination. Furthermore, to increase the internal surface area and light-harvesting efficiency, three-dimensional (3D) nanostructures have been introduced in QDSSCs.[24] Among 3D nanostructures, hybrid hierarchical nanostructures such as TiO₂/TiO₂-,[24] ZnO/ZnO-,[29,30] TiO₂/ZnO-,[31,32] SnO₂/TiO₂-,[33,34] and ZnO/Zn₂SnO₄-based[35,36] QDSSCs or DSSCs exhibited excellent photovoltaic performance. Compared with the mostly used TiO₂, ZnO seems to be a good alternative candidate for not only similar band gap (∼3.2 eV) and physical properties but also faster electron mobility than TiO₂ (205−1000 cm² V⁻¹ s⁻¹ for ZnO compared with 0.1−4 cm² V⁻¹ s⁻¹ for TiO₂).[37,38] However, the intriguing combination of ZnO and TiO₂ would be the best option to fabricate an efficient photoanode with

synergistic and complementary advantages. To the best of our knowledge, no work has been published on the vertically aligned hierarchical TiO_2 nanowire (TNW)/ZnO nanorod (ZNR) or TNW/ZnO nanosheet (ZNS) hybrid array-based QDSSCs.

In this study, we introduce novel vertically aligned TiO_2/ZnO hybrid arrays consisting of TNW on fluorine-doped tin oxide (FTO) glass coated with ZNR or ZNS via a two-step hydrothermal process, which are further used as photoanodes for efficient CdS/CdSe cosensitized solar cells. The photovoltaic performance of TNW/ZNS hybrid-heterostructure-based QDSSCs (3.57%) and TNW/ZNR-based QDSSCs (3.20%) is 30% and 17% higher than that of the smooth TNW-based QDSSCs (2.74%), respectively. Such a superior enhancement in the power conversion efficiency (PCE) can be attributed to larger surface area and higher light-harvesting efficiency for TiO_2/ZnO hybrid array heterostructures. Moreover, through utilization of a Cu_2S counter electrode, an optimized photovoltaic performance as high as 4.57% is achieved.

2. EXPERIMENTAL SECTION

2.1. Synthesis of Vertically Aligned TNW Arrays. First, a FTO substrate (2.5 cm × 3 cm) was ultrasonically cleaned with acetone, ethanol, and water for 10 min, respectively. Then, the TiO_2 compact layer was spin-coated on the cleaned FTO glass using a TiO_2 colloid solution,[39] followed by heating at 500 °C in ambient air for 30 min. Vertically aligned TNW arrays were prepared via a facile solution-processed method.[40] Briefly, 0.35 g of $K_2TiO(C_2O_4)_2$ was added to the mixture solvent containing 5 mL of water and 15 mL of diethylene glycol. After stirring for 30 min, the TiO_2 seed-layer-coated FTO was immersed in the solvent against the wall of the Teflon liner with its conducting side face down. The hydrothermal reaction was kept at 180 °C for 6 h. Afterward, the autoclave was cooled to room temperature naturally, and the as-synthesized vertically aligned TiO_2 arrays were rinsed with deionized water and ethanol and then dried at room temperature.

2.2. Synthesis of TNW/ZNR or ZNS Hybrid Arrays. To obtain the vertically aligned TNW/ZnO hybrid arrays, the above TNW array film was immersed in the ZnO solution[36] at room temperature for 30 min and then heated to 300 °C for 30 min, which resulted in the ZnO seed layer coating on the TNW surface. After that, the ZnO-seeded TNW arrays were immersed in a solution containing 0.1 M $Zn(NO_3)_2$, 0.1 M hexamethylenetetramine, 0.01 M sodium citrate, and 20 mL of deionized water at 90 °C for 3 h, which led to the formation of TNW/ZNS hybrid arrays. In contract, in the absence of sodium citrate, TNW/ZNR hybrid arrays were obtained.

2.3. Electrodeposition of CdS/CdSe QDs. Prior to electrodeposition, the as-prepared TiO_2/ZnO hybrid arrays were treated with a surface passivation solution that had been modified according to that reported in ref 37. Briefly, the as-synthesized TNW arrays and TNW/ZNS and TNW/ZNR hybrid heterostructured arrays were immersed in an aqueous solution containing 0.05 M H_3BO_3 and 0.05 M $(NH_4)_2TiF_6$ at room temperature for 30 min, washed with deionized water and ethanol, and then sintered at 500 °C for 30 min. The electrodeposition condition of CdS and CdSe QDs was reported in our previous study.[41] Briefly, for electrodeposition of CdS QDs, the electrolyte containing 0.2 M $Cd(NO_3)_2$, 0.2 M $CS(NH_2)_2$, and 1:1 (v/v) dimethyl sulfoxide/water was maintained at 90 °C for 18 min with a constant current of 0.625 mA cm^{-2}. The electrode was taken out, followed by rinsing with deionized water and ethanol successively. For the electrodeposition of CdSe QDs, the electrolyte contained 0.02 M $Cd(CH_3COO)_2$, 0.04 M ethylenediaminetetraacetic acid disodium salt, and 0.02 M Na_2SeSO_3 (prepared by refluxing 0.24 g of selenium powder and 1.0 g of Na_2SO_3 in water at 100 °C for 3 h) with a solution pH of 7.5−8. The electrodeposion was conducted at room temperature for 28 min with a constant current of 0.625 mA cm^{-2}.

2.4. Fabrication of TiO_2/ZnO Hybrid Array-Based QDSSCs. The vertically aligned TiO_2/ZnO hybrid arrays grown on FTO glass were used as photoanodes for QDSSCs. In order to evaluate the photovoltaic performance, the photoanodes were assembled with a platinum or Cu_2S counter electrode in a sandwich type, and the polysulfide electrolyte was injected into the space. The platinum counter electrode and polysulfide electrolyte containing 1 M Na_2S, 1 M sulfur, and 0.1 M NaOH in 7:3 (v/v) methanol/water were the same as those in our previous report.[41] The Cu_2S counter electrode was synthesized through facile chemical bath deposition. A total of 0.24 g of $CuSO_4$ was dissolved in 60 mL of deionized water, and then N_2 was bubble through the solution for 10 min to prevent the presence of oxygen in water. Then, 0.37 g of $Na_2S_2O_3·5H_2O$ was added to the system, forming a light-green solution, which was kept in a 90 °C water bath for 1 h. After that, the Cu_2S counter electrode was rinsed with deionized water and dried in ambient air.

2.5. Characterization. The morphology and structure of TiO_2/ZnO hybrid heterostructures were characterized by field-emission scanning electron microscopy (SEM; JSM-6330F) and transmission electron microscopy (TEM; JEOL-2010 HR). The phase structure of the sample was characterized on a Bruker D8 Advance X-ray diffractometer using Cu $K\alpha$ radiation (λ = 1.5418 Å). The diffuse-reflectance spectra were performed on a UV−vis−near-IR spectrophotometer (UV-3150). The photovoltaic performance of QDSSCs was characterized by a Keithley 2400 sourcemeter using a solar light simulator (Oriel model 91192) to simulate AM 1.5G illumination (100 mW cm^{-2}). The intensity was calibrated with a NREL-calibrated silicon solar cell. The incident photon-to-current conversion efficiency (IPCE) spectra were measured by a Keithley 2000 multimeter incorporated with a Spectral Product DK240 monochromator. The electrochemical impedance spectroscopy (EIS) spectra were measured by an electrochemical workstation (Zahner, Zennium) at a bias potential of −0.5 V in a frequency range from 10 mHz to 1 MHz under dark conditions. Intensity-modulated photocurrent/photovoltage spectroscopy (IMPS/IMVS) was also measured on the same electrochemical workstation under a modulated green-light-emitting diode (457 nm) with the frequency ranging from 100 kHz to 100 mHz. Also, IMPS and IMVS were measured at short-circuit and open-circuit conditions, respectively.

3. RESULTS AND DISCUSSION

3.1. Preparation Process, Morphology, X-ray Diffraction (XRD) Patterns, and Diffuse-Reflectance Spectra of TiO_2 Arrays and TiO_2/ZnO Hybrid Heterostructures. Figure 1 displays a schematic diagram of the step-by-step synthesis route to fabricate the TNW backbone and TNW/ZNS and TNW/ZNR hybrid arrays. All of the TiO_2/ZnO heterostructures were fabricated via a simple seed-assisted hydrothermal process. Interestingly, in the presence of sodium citrate, the TNW/ZNS hybrid arrays with lamellar nanosheets
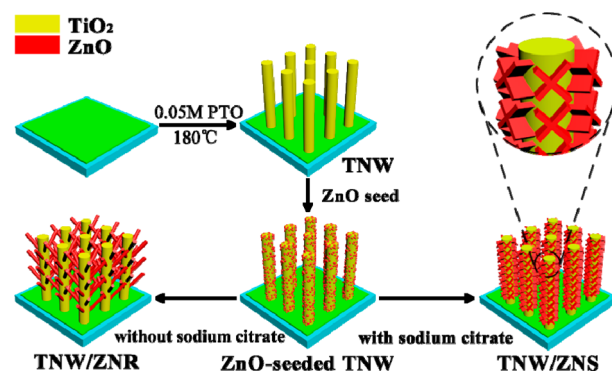

Figure 1. Schematic diagram of the step-by-step synthesis route to fabricate TNW/ZNS and TNW/ZNR hybrid arrays.

epitaxially grown on the surface of TNW backbones were obtained, while in the absence of sodium citrate, the rodlike ZnO was intelligently coated on the TNW scaffolds to form a treelike morphology. The schematic illustrations and relevant cross-sectional SEM images of TNW arrays and TNW/ZNR and TNW/ZNS hybrid arrays at low and high magnifications are shown in Figure 2. One can notice that all TiO$_2$ or TiO$_2$/
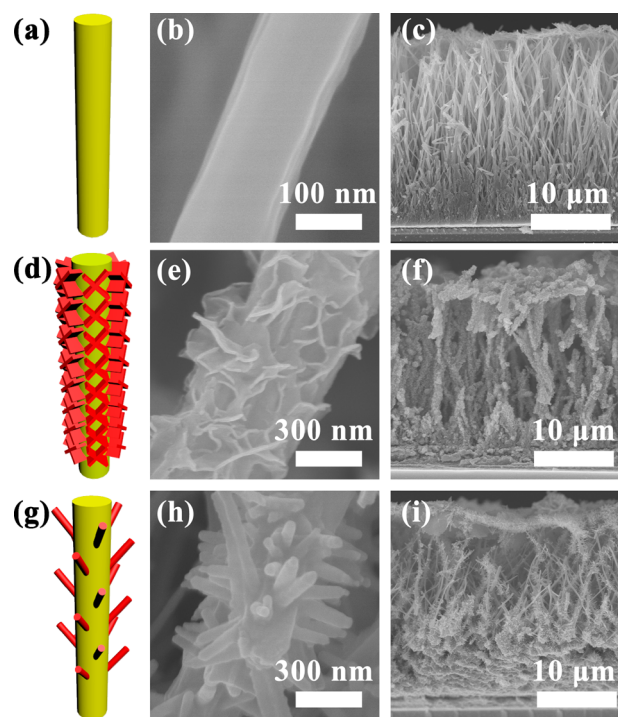

Figure 2. Schematic illustrations and cross-sectional SEM images of the as-synthesized TNW arrays (a−c) and TNW/ZNS (d−f) and TNW/ZNR hybrid arrays (g−i).

ZnO hybrid arrays grew perpendicularly on FTO glass with approximately ∼18 μm length (Figure 2c,f,i), which reveals that the thickness of the vertically aligned array film did not change even after subsequent ZnO modification. It is noted that the individual TNW shown in Figure 2b is very smooth, and such a structure is believed to exhibit a direct electric pathway for fast electron transport. However, the smooth surface is also related to a low internal surface area, leading to insufficient sensitizer anchoring and thus a limited photocurrent density when applied as a photoelectrode in solar cells.[40] In the current work, 1D ZNRs or 2D ZNSs are grown on the surface of the smooth TNW array backbone, for the sake of optimizing the physical, optical, and photoelectrochemical properties of array materials. After seeded with a ZnO solution to form a uniform ZnO seed layer for subsequent growth,[36] the TNW arrays went through a second-step facile hydrothermal reaction, which formed the TNW/ZNS or TNW/ZNR hybrid heterostructured arrays. The ZNSs (10−30 nm in thickness and 200 nm in length) germinated on TNW backbone arrays are shown in Figure 2c, while ZNRs (40−50 nm in diameter and 250 nm in length) coated on TNW backbone arrays are shown in Figure 2b. Interestingly, the significant difference between the growth of TNW/ZNS and TNW/ZNR hybrid heterostructured arrays only depended on the presence or absence of sodium citrate in the hydrothermal precursor solution (seen in the Experimental Section). It is worth noting that the emergence of sheetlike

ZnO branches can be attributed to the combination of sodium citrate and the (001) plane of the ZnO crystal during the hydrothermal process, which would suppress the growth of the ZnO crystal along the (001) plane.[30] Instead, ZnO can grow along its (001) axis in the absence of sodium citrate, leading to rodlike branches. The phase purity of the TNW arrays, TiO$_2$/ZnO hybrid arrays, and their CdS/CdSe QD-sensitized derivatives is characterized by XRD measurement (seen in Figure S1 in the Supporting Information, SI). Specifically, the TNW arrays can be indexed as pure anatase TiO$_2$ (JCPDS no. 21-1272).[40] As for the TNW/ZNS and TNW/ZNR hybrid heterostructures, additional peaks, which correspond to the characteristic signal of ZnO, can be observed. Such peaks can be indexed as the (100), (002), and (101) planes of crystalline ZnO (green rhombus shown in Figure S1 in the SI; JCPDS no. 65-3411). In addition, the QDs@TNW/ZNS and QDs@TNW/ZNR samples in the XRD pattern exhibit wide peaks at 42° and 44°, which can be ascribed to the subsequent electrodeposition of CdS and CdSe QDs. The wide peaks at 42° and 44° can be indexed to the (208) facet of cubic CdS (JCPDS no. 65-2887) and the (220) facet of cubic CdSe (JCPDS no. 65-2891), respectively.

The intrinsic morphology and structure characteristics are further confirmed by TEM, as shown in Figure 3. Figure 3a is
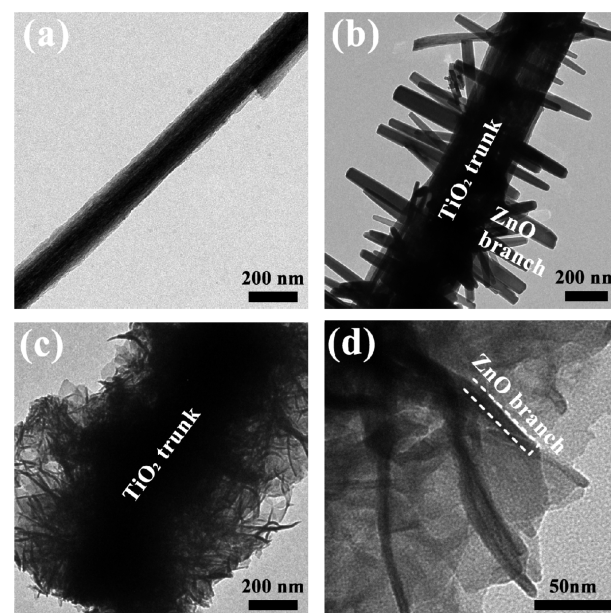

Figure 3. TEM images of the as-synthesized TNW arrays (a) and TNW/ZNR (b) and TNW/ZNS (c and d) hybrid arrays.

the TEM image of a TNW array sample showing a smooth morphology. The TNW/ZNS (Figure 3c,d) sample displays the epitaxial and lamellar nanosheets uniformly covering the surface of a pristine TNW backbone. On the other hand, the adjacent nanosheets also connect with each other and form an interconnected network with high porosity. Such geometry would be beneficial to electrolyte penetration. Figure 3b shows the morphology of TNW/ZNR hybrid heterostructures exhibiting a lower density of branches, which may lead to lower photovoltaic performance (low current density and open voltage) compared to TNW/ZNS hybrid heterostructures.

The diffuse-reflectance spectra of TNW arrays and TNW/ZNS and TNW/ZNR hybrid arrays are shown in Figure 4. Not
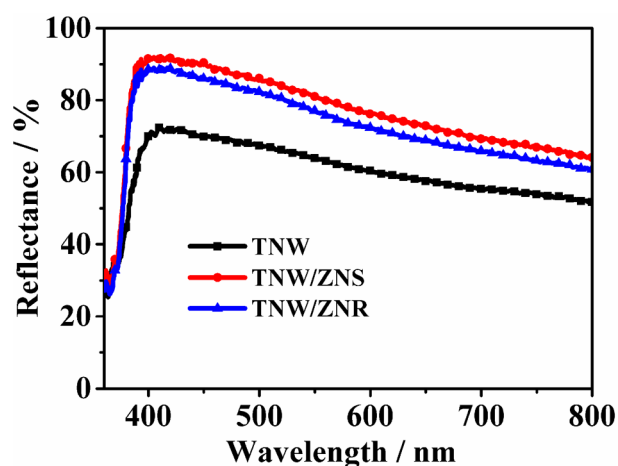
Figure 4. Diffuse-reflectance spectra of TNW arrays and TNW/ZNS and TNW/ZNR hybrid arrays.

Figure 5. (a) $J-V$ characteristics and (b) IPCE spectra of TNW arrays and TNW/ZNS and TNW/ZNR hybrid array-based QDSSCs.

surprisingly, the branched TiO_2/ZnO hybrid heterostructured arrays all exhibit higher reflectance than the smooth TNW arrays in the overall wavelength range from 380 to 800 nm, revealing that the branches grown on the TNW backbone largely improve light scattering for the array films. However, it is worth noting that the TNW/ZNS hybrid heterostructured arrays showcase better light-scattering capability than their TNW/ZNR counterparts, which may result from the 2D sheetlike branch morphology as well as higher density of branches germinated on the TNW backbone (as seen from SEM and TEM analysis).

3.2. Photovoltaic Performance and IPCE of TNW Arrays and TiO_2/ZnO Hybrid Heterostructured Array-Based QDSSCs. In order to illustrate the superior photovoltaic performance of the TiO_2/ZnO hybrid heterostructured arrays, TNW, TNW/ZNS, and TNW/ZNR arrays were applied as photoanodes in QDSSCs. The typical photocurrent density–photovoltage ($J-V$) curves of QDSSCs based on photoanodes of the TNW arrays and TNW/ZNS and TNW/ZNR hybrid arrays are shown in Figure 5a. The detailed parameters of the short-circuit photocurrent density (J_{sc}), open-circuit photovoltage (V_{oc}), fill factor (FF), and PCE (η) of TNW, TNW/ZNS, and TNW/ZNR arrays are summarized in Table 1. Clearly, all of the TiO_2/ZnO hybrid array-based QDSSCs exhibit better photovoltaic performance than the pristine TNW array counterparts. Specifically, TNW/ZNS hybrid heterostructured array-based QDSSCs exhibit the best photovoltaic performance of 3.57%, which is almost 30% higher than the smooth TNW array-based QDDSCs (2.74%). Also, TNW/ZNR hybrid heterostructured array-based QDSSCs exhibit a photovoltaic performance of 3.20%, which is almost 17% higher than the smooth TNW array-based QDSSCs. In detail, J_{sc} increased from 10.82 mA cm^{-2} (TNW) to 12.49 mA cm^{-2} for TNW/ZNR and further to 14.23 mA cm^{-2} for TNW/ZNS, which can be partially due to enhanced light-scattering capability (Figure 4), higher charge mobility of ZnO branches, and better light absorption (Figure S2 in the SI) for branched TiO_2/ZnO hybrid array photoanodes. It is noted that J_{sc} of TNW/ZNS-based QDSSCs is better than that of TNW/ZNR-based QDSSCs owing to the superior light scattering (Figure 4) and much more efficient light absorption after deposition of CdS/CdSe QDs (Figure S2 in the SI). V_{oc} decreased from 539 mV (TNW) to 504 mV (TNW/ZNS) to 493 mV (TNW/
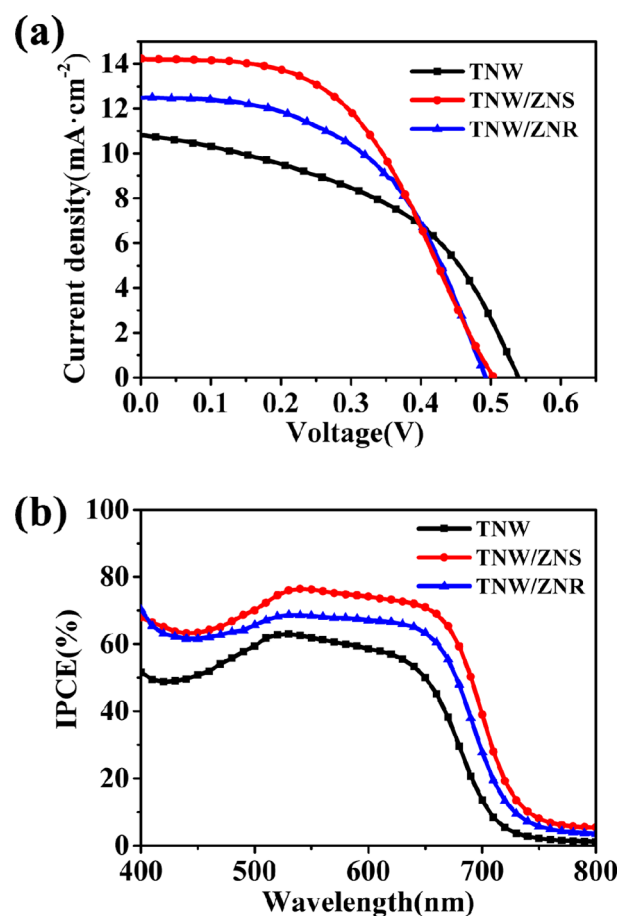
ZNR), which can be ascribed to the aggravated charge recombination resulting from the additional growth of ZnO branches. However, FF increased from 0.47 (TNW) to 0.52 (TNW/ZNR) to 0.50 (TNW/ZNS) primarily because of the improved connection between the roots of the arrays and the FTO glass after the second-step hydrothermal reaction (Figure S3 in the SI). It is worth noting that the ZNR or ZNS coverage on the TNW backbone just occurred in the absence or presence of sodium citrate. For QDSSC applications, we have observed significantly increased J_{sc} for TNW/ZNS cells, which is higher than that of the TNW/ZNR analogue, while V_{oc} and FF are similar for these two cells. The improved J_{sc} for TNW/ZNS cells can be attributed to superior light scattering and light trapping for improved light harvesting. To further evaluate the photovoltaic performance of QDSSCs, the monochromatic IPCE spectra, which highly correspond to the photocurrent density of the QDSSCs, were measured as a function of the wavelength ranging from 400 to 800 nm (shown in Figure 5b). Obviously, the IPCE values of QDSSCs based on TiO_2/ZnO hybrid array photoanodes are higher than those of pristine

Table 1. Detailed Photovoltaic Parameters of QDSSCs Based on Different Photoanodes and Counter Electrodes

QDSSC	J_{sc} (mA cm^{-2})	V_{oc} (mV)	η (%)	FF
TNW	10.82	539	2.75	0.47
TNW/ZNR	12.49	493	3.20	0.52
TNW/ZNS	14.23	504	3.57	0.50
TNW/ZNS-Cu$_2$S	16.11	512	4.57	0.55

TNW counterparts in the whole wavelength. The highest IPCE values at around 530 nm are 63.1%, 68.7%, and 76.4% for TNW, TNW/ZNR, and TNW/ZNS, respectively, which is in accordance with the photocurrent density shown in Table 1. It is notable that an obvious red-shift phenomenon is observed for TiO$_2$/ZnO hybrid heterostructured array-based QDSSCs at a longer wavelength range from 650 to 750 nm, owing to the enhanced capability of light scattering and utilization at this wavelength region compared to TNW-based QDSSCs. This fact is best illustrated by the diffuse-reflectance spectra (shown in Figure 4).

3.3. EIS Studies and Charge-Transfer and Recombination Dynamic Analysis of TiO$_2$ Arrays and TiO$_2$/ZnO Hybrid Heterostructured Array-Based QDSSCs.

To further investigate the dynamics of charge transport and recombination within QDSSCs based on TNW, TNW/ZNS, and TNW/ZNR arrays, EIS studies were carried out. Figure 6a
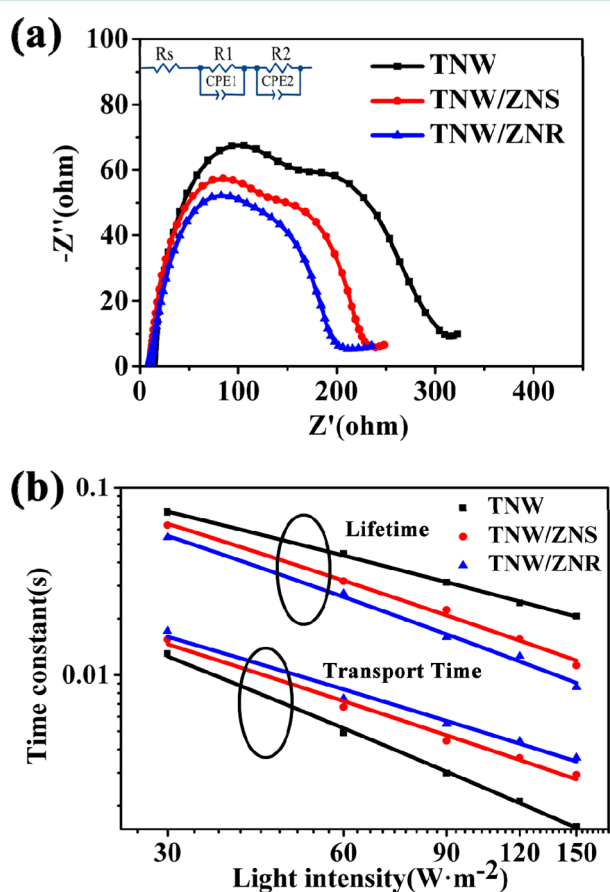

Figure 6. (a) EIS spectra and (b) IMPS/IMVS results of QDSSCs based on TNW arrays TNW/ZNS and TNW/ZNR hybrid arrays.

shows the Nyquist curve from EIS spectra, and the corresponding stimulated series resistance (R_s), charge-transfer resistance (R_1) for the electron-transfer process at the counter electrode/electrolyte interface (the first semicircle), recombination resistance (R_2) for the electron-transfer process at the semiconductor arrays/QDs/electrolyte interface (the second semicircle), and electron lifetime (τ_r) are summarized in Table S1 in the SI. It is worth noting that R_s of TNW/ZNS and TNW/ZNR hybrid arrays is higher than that of TNW arrays, leading to enhanced FF for such cells, which is caused by the aforementioned improved contact between hybrid arrays and

the front electrode (shown in Figure S3 in the SI). On the other hand, the recombination resistance (R_2) decreased from 198.9 Ω (TNW) to 178.1 Ω (TNW/ZNS) to 140.6 Ω (TNW/ZNR), and the electron lifetime (τ_r) decreased from 72.3 ms (TNW) to 45.9 ms (TNW/ZNS) to 26.3 ms (TNW/ZNR), indicating much more charge recombination within the hybrid array-based cells, which is strongly related to the additional growth of ZnO branches and thus inevitably introduced additional boundaries, defects, and trapped/detrapped events for recombination. Under such circumstances, the declined V_{oc} is in good accordance with the decreased electron lifetime.

In addition, to further characterize the electron transportation and charge recombination within the films of TNW, TNW/ZNS, and TNW/ZNR, IMPS and IMVS measurements were conducted. Figure 6b shows the electron-transport time (τ_d) and electron lifetime (τ_r) for TNW-, TNW/ZNS-, and TNW/ZNS-based QDSSCs, where τ_d represents the transit time of the photogenerated electron within the photoanode films, while τ_r represents the recombination time of electrons with S_n^{2-} in the electrolyte, which can be calculated by IMPS and IMVS plots using the expressions $\tau_d = 1/2\pi f_d$ and $\tau_r = 1/2\pi f_r$, in which f_d and f_r stand for the characteristic minimum frequency of the IMPS and IMVS imaginary components, respectively.[41] As shown in Figure 6b, the TNW-based QDSSCs have higher τ_r and lower τ_d than the TiO$_2$/ZnO-based QDSSCs, indicating a faster transport rate and a slower recombination rate for the TNW-based QDSSCs, from which we can conclude that the introduction of ZnO nanobranches would prolong the charge-transport pathway and, moreover, the enlarged surface area would bring about additional recombination centers for serious charge recombination, leading to hindered electron transport and shorted electron lifetime and thus inferior charge collection. However, although TiO$_2$/ZnO hybrid array-based QDSSCs suffer from a decrease of V_{oc}, their significant improvement of J_{sc} and FF offers great contribution to the improvement of the photovoltaic efficiency, which, consequently, exhibits 30% higher PCE for ZNS/TNW hybrid heterostructured array-based QDSSCs compared to TNW-based QDSSCs.

3.4. Photovoltaic Performance and EIS Studies of TNW/ZNS Hybrid Heterostructured Array-Based QDSSCs Assembled with Platinum and Cu$_2$S Counter Electrodes.

The platinum counter electrodes have poor electrocatalytic activities in the polysulfide electrolyte, which cause higher resistance and lower QD regeneration rate.[42] Therefore, a thin film of Cu$_2$S on FTO glass as the counter electrode is introduced via a simple and facile chemical bath deposition. With the as-synthesized Cu$_2$S counter electrode, we fabricate the TNW/ZNS-based QDSSCs, and the detailed photovoltaic performance compared with that of the QDSSCs based on a platinum counter electrode is summarized in Table 1. The typical $J-V$ curve is shown in Figure 7a. To further characterize the dynamics of charge transport and recombination within QDSSCs based on platinum and Cu$_2$S counter electrodes, EIS studies were carried out, which are shown in Figure 7b. As a result, QDSSCs based on a Cu$_2$S counter electrode further improve the photovoltaic performance, and an impressive PCE as high as 4.57% was achieved (J_{sc} = 16.11 mA cm^{-2}, V_{oc} = 512 mV, and FF = 0.55), 28% higher than that of their platinum-based counterparts (J_{sc} = 14.23 mA cm^{-2}, V_{oc} = 504 mV, and FF = 0.50). This result is attributed to the superior electrocatalytic capabilities and lower charge resistance
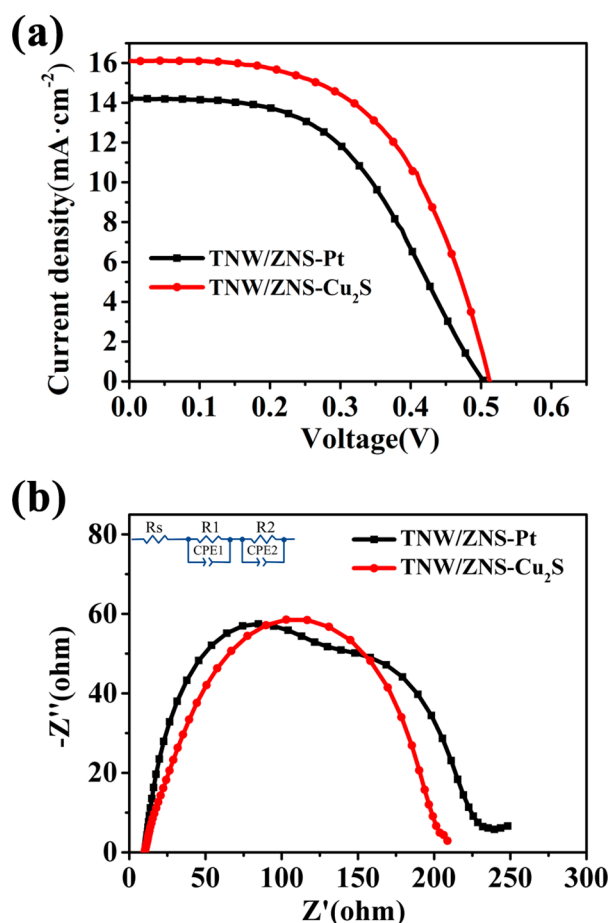
(a)

(b)

Figure 7. (a) *J−V* characteristics and (b) EIS spectral results of TNW/ZNS hybrid array-based QDDSCs with a platinum or Cu$_2$S counter electrode.

(R_1 = 13.84 Ω for the Cu$_2$S counter electrode compared to 146.7 Ω for the platinum counter electrode).

4. CONCLUSION

In summary, novel vertically aligned TNW/ZNR or ZNS hybrid heterostructured arrays on FTO glass had been successfully synthesized by facile, cheap, and green hydrothermal processes for highly efficient QDSSCs. The as-synthesized TiO$_2$/ZnO hybrid arrays exhibited optimized light harvesting compared to that of pristine TNW arrays. Consequently, TNW/ZNS hybrid array-based QDSSCs exhibited a promising PCE of 4.57% with an optimized Cu$_2$S counter electrode. The present work demonstrates the possibility of fabricating vertically aligned arrays with heterostructured architecture via a simple hydrothermal protocol, which we believe will potentially exhibit significant performances in various areas such as organic−inorganic hybrid perovskite solar cells, water splitting, lithium-ion batteries, fuel cells, supercapacitors, field emission, etc.

■ ASSOCIATED CONTENT

Ⓢ Supporting Information

XRD patterns, UV−vis absorption spectra, cross-sectional SEM image, and detailed simulative value from EIS spectra. This material is available free of charge via the Internet at http://pubs.acs.org.

■ AUTHOR INFORMATION

Corresponding Author
*E-mail: kuangdb@mail.sysu.edu.cn. Fax: (+86) 20-8411 3015.
Notes
The authors declare no competing financial interest.

■ ACKNOWLEDGMENTS

■ REFERENCES

(1) O'Regan, B.; Grätzel, M. A Low-cost, High-efficiency Solar Cell Based on Dye-sensitized Colloidal TiO$_2$ Films. *Nature* **1991**, *353*, 737−740.

(2) Grätzel, M. Photoelectrochemical Cells. *Nature* **2001**, *414*, 338−344.

(3) Chen, X.; Mao, S. S. Titanium Dioxide Nanomaterials: Synthesis, Properties, Modifications, and Applications. *Chem. Rev.* **2007**, *107*, 2891−2959.

(4) Yella, A.; Lee, H. W.; Tsao, H. N.; Yi, C. Y.; Chandiran, A. K.; Nazeeruddin, M. K.; Diau, E. W. G.; Yeh, C. Y.; Zakeeruddin, S. M.; Grätzel, M. Porphyrin-Sensitized Solar Cells with Cobalt(II/III)-Based Redox Electrolyte Exceed 12% Efficiency. *Science* **2011**, *334*, 629−634.

(5) Hagfeldt, A.; Boschloo, G.; Sun, L.; Kloo, L.; Pettersson, H. Dye-sensitized Solar cells. *Chem. Rev.* **2010**, *110*, 6595−6663.

(6) Wu, W. Q.; Xu, Y. F.; Rao, H. S.; Su, C. Y.; Kuang, D. B. Multistack Integration of Three-dimensional Hyperbranched Anatase Titania Architectures for High-efficiency Dye-sensitized solar cells. *J. Am. Chem. Soc.* **2014**, *136*, 6437−6445.

(7) Mathew, S.; Yella, A.; Gao, P.; Humphry-Baker, R.; Curchod, B. F. E.; Ashari-Astani, N.; Tavernelli, I.; Rothlisberger, U.; Nazeeruddin, M. K.; Grätzel, M. Dye-sensitized Solar Cells with 13% Efficiency Achieved through the Molecular Engineering of Porphyrin Sensitizers. *Nat. Chem.* **2014**, *6*, 242−247.

(8) Pan, Z.; Mora-Sero, I.; Shen, Q.; Zhang, H.; Li, Y.; Zhao, K.; Wang, J.; Zhong, X.; Bisquert, J. High-efficiency "Green" Quantum Dot Solar Cells. *J. Am. Chem. Soc.* **2014**, *136*, 9203−9210.

(9) Sun, W. T.; Yu, Y.; Pan, H. Y.; Gao, X. F.; Chen, Q.; Peng, L. M. CdS Quantum Dots Sensitized TiO$_2$ Nanotube-array Photoelectrodes. *J. Am. Chem. Soc.* **2008**, *130*, 1124−1125.

(10) Baker, D. R.; Kamat, P. V. Photosensitization of TiO$_2$ Nanostructures with CdS Quantum Dots: Particulate versus Tubular Support Architectures. *Adv. Funct. Mater.* **2009**, *19*, 805−811.

(11) Leschkies, K. S.; Divakar, R.; Basu, J.; Enache-Pommer, E.; Boercker, J. E.; Carter, C. B.; Kortshagen, U. R.; Norris, D. J.; Aydil, E. S. Photosensitization of ZnO Nanowires with CdSe Quantum Dots for Photovoltaic Devices. *Nano Lett.* **2007**, *7*, 1793−1798.

(12) Lee, H.; Wang, M. K.; Chen, P.; Gamelin, D. R.; Zakeeruddin, S. M.; Grätzel, M.; Nazeeruddin, M. K. Efficient CdSe Quantum Dot-Sensitized Solar Cells Prepared by an Improved Successive Ionic Layer Adsorption and Reaction Process. *Nano Lett.* **2009**, *9*, 4221−4227.

(13) Gao, X. F.; Li, H. B.; Sun, W. T.; Chen, Q.; Tang, F. Q.; Peng, L. M. CdTe Quantum Dots-Sensitized TiO$_2$ Nanotube Array Photoelectrodes. *J. Phys. Chem. C* **2009**, *113*, 7531−7535.

(14) Bang, J. H.; Kamat, P. V. Quantum Dot Sensitized Solar Cells. A Tale of Two Semiconductor Nanocrystals: CdSe and CdTe. *ACS Nano* **2009**, *3*, 1467−1476.

(15) McDonald, S. A.; Konstantatos, G.; Zhang, S. G.; Cyr, P. W.; Klem, E. J. D.; Levina, L.; Sargent, E. H. Solution-processed PbS Quantum Dot Infrared Photodetectors and Photovoltaics. *Nat. Mater.* **2005**, *4*, 138−142.

(16) Hyun, B. R.; Zhong, Y. W.; Bartnik, A. C.; Sun, L. F.; Abruna, H. D.; Wise, F. W.; Goodreau, J. D.; Matthews, J. R.; Leslie, T. M.;

Borrelli, N. F. Electron Injection from Colloidal PbS Quantum Dots into Titanium Dioxide Nanoparticles. *ACS Nano* **2008**, *2*, 2206−2212.

(17) Long, R.; Prezhdo, O. V. Ab Initio Nonadiabatic Molecular Dynamics of the Ultrafast Electron Injection from a PbSe Quantum Dot into the TiO$_2$ Surface. *J. Am. Chem. Soc.* **2011**, *133*, 19240−19249.

(18) Boix, P. P.; Larramona, G.; Jacob, A.; Delatouche, B.; Mora-Sero, I.; Bisquert, J. Hole Transport and Recombination in All-Solid Sb$_2$S$_3$-Sensitized TiO$_2$ Solar Cells Using CuSCN as Hole Transporter. *J. Phys. Chem. C* **2012**, *116*, 1579−1587.

(19) Kongkanand, A.; Tvrdy, K.; Takechi, K.; Kuno, M.; Kamat, P. V. Quantum Dot Solar Cells: Tuning Photoresponse through Size and Shape Control of CdSe−TiO$_2$ Architecture. *J. Am. Chem. Soc.* **2008**, *130*, 4007−4015.

(20) Yu, W. W.; Qu, L. H.; Guo, W. Z.; Peng, X. G. Experimental Determination of the Extinction Coefficient of CdTe, CdSe, and CdS Nanocrystals. *Chem. Mater.* **2003**, *15*, 2854−2860.

(21) Sambur, J. B.; Novet, T.; Parkinson, B. A. Multiple Exciton Collection in a Sensitized Photovoltaic System. *Science* **2010**, *330*, 63−66.

(22) Klimov, V. I. Mechanisms for Photogeneration and Recombination of Multiexcitons in Semiconductor Nanocrystals: Implications for Lasing and Solar Energy Conversion. *J. Phys. Chem. B* **2006**, *110*, 16827−16845.

(23) Hanna, M. C.; Nozik, A. J. Solar Conversion Efficiency of Photovoltaic and Photoelectrolysis Cells with Carrier Multiplication Absorbers. *J. Appl. Phys.* **2006**, *100*, 074510.

(24) Rao, H. S.; Wu, W. Q.; Liu, Y.; Xu, Y. F.; Chen, B. X.; Chen, H. Y.; Kuang, D. B.; Su, C. Y. CdS/CdSe Co-sensitized Vertically Aligned Anatase TiO$_2$ Nanowire Arrays for Efficient Solar Cells. *Nano Energy* **2014**, *8*, 1−8.

(25) Xiao, J. Y.; Huang, Q. L.; Xu, J.; Li, C. H.; Chen, G. P.; Luo, Y. H.; Li, D. M.; Meng, Q. B. CdS/CdSe Co-Sensitized Solar Cells Based on a New SnO$_2$ Photoanode with a Three-Dimensionally Interconnected Ordered Porous Structure. *J. Phys. Chem. C* **2014**, *118*, 4007−4015.

(26) Wang, Y. F.; Li, K. N.; Xu, Y. F.; Su, C. Y.; Kuang, D. B. Hierarchical Zn$_2$SnO$_4$ Nanosheets Consisting of Nanoparticles for Efficient Dye-sensitized Solar Cells. *Nano Energy* **2013**, *2*, 1287−1293.

(27) Li, L.; Zhai, T.; Bando, Y.; Golberg, D. Recent Progress of One-dimensional ZnO Nanostructured Solar Cells. *Nano Energy* **2012**, *1*, 91−106.

(28) Qi, X. P.; She, G. W.; Liu, Y. Y.; Mu, L. X.; Shi, W. S. Electrochemical Synthesis of CdS/ZnO Nanotube Arrays with Excellent Photoelectrochemical Properties. *Chem. Commun.* **2012**, *48*, 242−244.

(29) Xu, F.; Dai, M.; Lu, Y.; Sun, L. Hierarchical ZnO Nanowire−Nanosheet Architectures for High Power Conversion Efficiency in Dye-Sensitized Solar Cells. *J. Phys. Chem. C* **2010**, *114*, 2776−2782.

(30) Tian, J. J.; Uchaker, E.; Zhang, Q. F.; Cao, G. Z. Hierarchically Structured ZnO Nanorods−Nanosheets for Improved Quantum-Dot-Sensitized Solar Cells. *ACS Appl. Mater. Interfaces* **2014**, *6*, 4466−4472.

(31) Bai, Y.; Yu, H.; Li, Z.; Amal, R.; Lu, G. Q.; Wang, L. Z. In Situ Growth of a ZnO Nanowire Network within a TiO$_2$ Nanoparticle Film for Enhanced Dye-Sensitized Solar Cell Performance. *Adv. Mater.* **2012**, *24*, 5850−5856.

(32) Ali, Z.; Shakir, I.; Kang, D. J. Highly Efficient Photoelectrochemical Response by Sea-urchin Shaped ZnO/TiO$_2$ Nano/micro Hybrid Heterostructures Co-sensitized with CdS/CdSe. *J. Mater. Chem. A* **2014**, *2*, 6474−6479.

(33) Ahn, S. H.; Kim, D. J.; Chi, W. S.; Kim, J. H. Hierarchical Double-Shell Nanostructures of TiO$_2$ Nanosheets on SnO$_2$ Hollow Spheres for High-Efficiency, Solid-State, Dye-Sensitized Solar Cells. *Adv. Funct. Mater.* **2014**, *24*, 5037−5044.

(34) Ahn, S. H.; Kim, D. J.; Chi, W. S.; Kim, J. H. One-Dimensional Hierarchical Nanostructures of TiO$_2$ Nanosheets on SnO$_2$ Nanotubes for High Efficiency Solid-State Dye-Sensitized Solar Cells. *Adv. Mater.* **2013**, *25*, 4893−4897.

(35) Bora, T.; Kyaw, H. H.; Dutta, J. Zinc Oxide−Zinc Stannate Core−shell Nanorod Arrays for CdS Quantum Dot Sensitized Solar Cells. *Electrochim. Acta* **2012**, *68*, 141−145.

(36) Li, L. B.; Wang, Y. F.; Rao, H. S.; Wu, W. Q.; Li, K. N.; Su, C. Y.; Kuang, D. B. Hierarchical Macroporous Zn$_2$SnO$_4$−ZnO Nanorod Composite Photoelectrodes for Efficient CdS/CdSe Quantum Dot Co-Sensitized Solar Cells. *ACS Appl. Mater. Interfaces* **2013**, *5*, 11865−11871.

(37) Tian, J. J.; Zhang, Q. F.; Uchaker, E.; Gao, R.; Qu, X. H.; Zhang, S. E.; Cao, G. Z. Architectured ZnO Photoelectrode for High Efficiency Quantum Dot Sensitized Solar Cells. *Energy Environ. Sci.* **2013**, *6*, 3542−3547.

(38) Tian, J.; Uchaker, E.; Zhang, Q.; Cao, G. Hierarchically Structured ZnO Nanorods−Nanosheets for Improved Quantum-dot-sensitized Solar Cells. *ACS Appl. Mater. Interfaces* **2014**, *6*, 4466−4472.

(39) Wang, Y. F.; Li, J. W.; Hou, Y. F.; Yu, X. Y.; Su, C. Y.; Kuang, D. B. Hierarchical Tin Oxide Octahedra for Highly Efficient Dye-Sensitized Solar Cells. *Chem.—Eur. J.* **2010**, *16*, 8620−8625.

(40) Wu, W. Q.; Lei, B. X.; Rao, H. S.; Xu, Y. F.; Wang, Y. F.; Su, C. Y.; Kuang, D. B. Hydrothermal Fabrication of Hierarchically Anatase TiO$_2$ Nanowire Arrays on FTO glass for Dye-sensitized Solar Cells. *Sci. Rep.* **2013**, *3*, 1352.

(41) Yu, X. Y.; Liao, J. Y.; Qiu, K. Q.; Kuang, D. B.; Su, C. Y. Dynamic Study of Highly Efficient CdS/CdSe Quantum Dot-Sensitized Solar Cells Fabricated by Electrodeposition. *ACS Nano* **2011**, *5*, 9494−9500.

(42) Jiang, Y.; Zhang, X.; Ge, Q. Q.; Yu, B. B.; Zou, Y. G.; Jiang, W. J.; Song, W. G.; Wan, L. J.; Hu, J. S. ITO@Cu$_2$S Tunnel Junction Nanowire Arrays as Efficient Counter Electrode for Quantum-Dot-Sensitized Solar Cells. *Nano Lett.* **2014**, *14*, 365−372.